INTEGR. COMP. BIOL., 42:971–980 (2002)

Flow Patterns Around the Carapaces of Rigid-bodied, Multi-propulsor Boxfishes (Teleostei: Ostraciidae)[1]

IAN K. BARTOL,[2]* MALCOLM S. GORDON,* MORTEZA GHARIB,† JAY R. HOVE,† PAUL W. WEBB,‡ AND DANIEL WEIHS§

*Department of Organismic Biology, Ecology, and Evolution, University of California, Los Angeles, California 91606
†Options of Bioengineering and Aeronautics, California Institute of Technology, Pasadena, California 91125
‡School of Natural Resources and Department of Biology, University of Michigan, Ann Arbor, Michigan 48109
§Department of Aerospace Engineering, Technion, Haifa, 3200, Israel

SYNOPSIS. Boxfishes (Teleostei: Ostraciidae) are rigid-body, multi-propulsor swimmers that exhibit unusually small amplitude recoil movements during rectilinear locomotion. Mechanisms producing the smooth swimming trajectories of these fishes are unknown, however. Therefore, we have studied the roles the bony carapaces of these fishes play in generating this dynamic stability. Features of the carapaces of four morphologically distinct species of boxfishes were measured, and anatomically-exact stereolithographic models of the boxfishes were constructed. Flow patterns around each model were investigated using three methods: 1) digital particle image velocimetry (DPIV), 2) pressure distribution measurements, and 3) force balance measurements. Significant differences in both cross-sectional and longitudinal carapace morphology were detected among the four species. However, results from the three interrelated approaches indicate that flow patterns around the various carapaces are remarkably similar. DPIV results revealed that the keels of all boxfishes generate strong longitudinal vortices that vary in strength and position with angle of attack. In areas where attached, concentrated vorticity was detected using DPIV, low pressure also was detected at the carapace surface using pressure sensors. Predictions of the effects of both observed vortical flow patterns and pressure distributions on the carapace were consistent with actual forces and moments measured using the force balance. Most notably, the three complementary experimental approaches consistently indicate that the ventral keels of all boxfishes, and in some species the dorsal keels as well, effectively generate self-correcting forces for pitching motions—a characteristic that is advantageous for the highly variable velocity fields in which these fishes reside.

INTRODUCTION

The marine boxfishes (Teleostei: Ostraciidae) are mostly shallow-water, tropical reef-dwelling fishes that have 2/3–3/4 of their bodies encased in rigid bony carapaces, which are keeled with various protuberances (Tyler, 1980; Nelson, 1994). As a result, many boxfishes cannot bend their bodies anterior to their caudal peduncles, and almost all of their swimming movements derive from complex combinations of motions of their five fins. Field observations and recent studies on the swimming physiology of boxfishes indicate that they are capable of remarkably low recoil motions, resulting in smooth, energy-efficient swimming trajectories that do not compromise maneuverability (Gordon *et al.*, 2000; Hove *et al.*, 2001). Although there are some studies describing and analyzing swimming in rigid-bodied ostraciiform fishes (Blake, 1977, 1981, 1983*a*, *b*; Hove *et al.*, 2001), little is known about how this remarkable stability is achieved. One goal of our work is to understand what role the body, which varies considerably in shape among the different species of ostraciids, plays in maintaining this stability, and, in particular, pitch control.

Because detailed data on the body shapes of ostraciiform fishes are lacking, we began by measuring major features of the carapaces of four morphologically distinct boxfishes: spotted boxfish *Ostracion meleagris*, smooth trunkfish *Lactophrys triqueter*, scrawled cowfish *Acanthostracion quadricornis*, and buffalo trunkfish *Lactophrys trigonus*. Next, using stereolithographic models of the carapaces of these four fishes, we performed three separate but interrelated experiments by different means to study flow around their bodies: digital particle image velocimetry (DPIV), surface pressure distributions, and force balance experiments. In this paper, we provide a general overview of the morphological measurements and above techniques, and highlight some important discoveries that elucidate the role the body plays in dynamic stability. A more in-depth treatment of these data may be found in Bartol *et al.*, 2002, 2003.

MATERIALS AND METHODS

Morphological measurements

Carapace characteristics were measured for six spotted boxfish *O. meleagris* (10.4–14.6 cm total length (TL), 30.5–71.1 g), eleven smooth trunkfish *L. triqueter* (14.7–23.0 cm TL, 94.8–368.0 g), six scrawled cowfish *A. quadricornis* (16.1–33.5 cm TL, 63.8–554.3 g), and four buffalo trunkfish *L. trigonus* (23.4–39.5 cm TL, 261.2–1,486.7 g). All measurements were collected from overanesthetized or frozen (−70°C) specimens. The locations of the centers of mass in the

[1] From the Symposium *Dynamics and Energetics of Animal Swimming and Flying* presented at the Annual Meeting of the Society for Integrative and Comparative Biology, 2–6 January 2002, at Anaheim, California.

[2] Present address of I. K. Bartol is MS#2, Woods Hole Oceanographic Institution, Woods Hole, MA 02543; E-mail: ibartol@whoi.edu

XY planes were estimated by first suspending fishes from three different positions on the body using monofilament line and a hook. A plumb line was aligned with the monofilament line for each of the three positions, and the paths of the plumb lines were drawn on the fish body using a marker. The points of intersection of the three lines located the centers of mass.

Using a Sony DCR-PC100 digital video camera, pictures of the fishes were taken from different perspectives, and various body characteristics were measured using NIH Image v. 1.61. The maximum height and width of each body and their corresponding locations relative to the snout were measured in lateral and ventral photographs, respectively. To characterize differences in keel morphology, the angles of dorsal and ventral keels at the locations of greatest body girth were recorded using photographs taken from anterior/posterior perspectives. Furthermore, to characterize the levels of lateral concavity or convexity of the sides, segments (S_L) connecting the apices of the ventral and dorsal keels were drawn on each side of the fish at the location of greatest girth using NIH Image. These segments were drawn in anterior and posterior photographs. The maximum distance the body indented and/or extended relative to the segment and the location of maximum indentation/extension along the segment were recorded. A similar procedure was used to characterize ventral (and dorsal for spotted boxfish) concavities/convexities, whereby reference segments either connected the apices of both ventral keels (S_V) or both dorsal keels (S_D).

Computerized Tomographic (CT) scanning

One specimen of each species was scanned using a GE CT/i high-speed scanner (General Electric Medical Systems, Milwaukee, WI). The CT scans were performed on either frozen (−70°C) or overanesthetized specimens with dorsal and anal fins removed and pectoral fins flush against the body. For each fish, 204–360 consecutive, 2-dimensional, cross-sectional exposures were generated longitudinally from the snout to the posterior edge of the caudal fin. Digital stereolithography (STL) files of the fishes were created using a Marching Cubes algorithm, a high-resolution 3D surface construction algorithm (Lorensen and Cline, 1987), and physical models of the fishes were created from the files using stereolithographic rapid-prototyping (Solid Concepts, Inc., Valencia, CA). Keel angle and body concavity/convexity measurements (described above) were recorded from CT scans at several locations along the body.

Digital Particle Image Velocimetry (DPIV)

Willert and Gharib (1991) and Raffel *et al.* (1998) provide detailed descriptions of the DPIV technique for flow field measurements. A brief general description of the experimental techniques relevant to our study is given here. To reduce glare from laser light, the models were painted black. The tails of the models were removed and replaced with a 0.5–1.0 cm diameter rod (the approximate diameter of the different caudal peduncles). The rod, which was 10 cm in length, was attached to a sting that entered the water tunnel from above. A water tunnel with a 30 × 30 × 100 cm test section (Model 503, Engineering Laboratory Design, Inc., Lake City, MN) seeded with silver-coated hollow glass spheres (14 μm in diameter) was used in the experiments. Two pulsed ND:YAG lasers (wavelength = 532 nm, power rating 50 mJ, [New Wave Research, Fremont, CA]), a series of front-surface mirrors, and a cylindrical lens were used to generate and align an illuminated sheet ~1.0 mm thick. The laser sheet was projected underneath the water tunnel in a transverse (YZ) plane. A Pulnix video camera (TM-9701) with a frame size of 460 × 768 pixels and frame rate of 30 Hz was positioned downstream of the working section (unobstructed views of oncoming flow was possible because of a Plexiglas exit tank).

The video camera, lasers, and a Coreco OC-TC10-DIGSE frame grabber (National Instruments, Inc., Austin, TX) were synchronized using a video timing box and *Flow Vision™* software (General Pixels, Pasadena, CA), allowing for the collection of a series of paired digital images. The interrogation window (*i.e.*, the area over which the particle shifts were averaged) was 32^2 pixels with a 16 pixel offset (50% overlap). The displacement of particles within paired images was calculated by cross-correlation (Willert and Gharib, 1991), and outliers, defined as particle shifts that were 3 or more pixels greater than particles shifts of neighboring particles, were removed and corrected. Velocity fields were determined by dividing flow displacement fields by the time difference between paired images. DPIV data were collected at various transverse sections along the models, which were positioned at various pitching angles of attack (−30 to +30°) in the water tunnel. Data were collected at 2° intervals between −10 and +10°, and at 5° intervals at more negative and positive angles of attack. The water tunnel was set at a speed of 44.0 cm sec^{-1} (1.9–2.6 body length sec^{-1}).

Pressure measurements

Boxfish models were hollowed out, and a series of 36–48 holes were drilled along dorsal, lateral, and ventral regions of each carapace. Urethane tubing (0.068 cm ID, 0.129 cm OD) was inserted into the holes and glued in place so that the tubing was flush with the model surface. Tubing exited the model through a 1.0 cm rod attached to a posterior section of the model. The rod was used to mount the model to a sting in a 61 cm wind tunnel (Model 407, Engineering Laboratory Design, Inc., Lake City, MN). The tubing was connected to a Scanivalve 48-channel rotating pressure scanner (Scanivalve Inc., Liberty Lake, WA) and a Barocel pressure transducer (Barocel Datametrics, Wilmington, MA). Static pressure at each of the 36–48 ports was expressed relative to static pressure at a tunnel wall port positioned perpendicular to flow. Data were collected while each model was positioned at 2°

intervals from angles of attack of −30 to +30°; for each of the 31 angles considered, data were acquired at 100 Hz for 10 sec using LabVIEW software (National Instruments, Inc.). Wind tunnel speed was set according to the Reynolds number considered in water tunnel trials. Pressure coefficients (C_p) were calculated by dividing the pressure difference above by dynamic pressure ($\rho U^2/2$; where ρ = air density and U is wind speed) determined using a Pitot tube positioned in the wind tunnel.

Force measurements

Each model was mounted caudally to a sting in a water tunnel with a test section 61 × 46 × 244 cm in dimension. Force measurements were collected using three Interface 5 lb strain gauge load cells (Interface, Inc. Scottsdale, AZ) (two load cells measured forces normal to flow [lift], one load cell measured forces parallel to flow [drag]) connected to an in-house force balance (Lisoski, 1993). Output from the load cells was amplified using three Interface SGA amplifiers/conditioners and was recorded using a Dash 8 Series data recorder (Astro-Med, Inc.). Data were collected at 200 Hz for 10 sec at each port for each angle considered. As was the case for pressure experiments, force data were collected every 2° from angles of attack of −30 to +30°. Flow speed during trials was identical to that considered in DPIV experiments (44.0 cm sec^{-1} [1.9–2.6 body length sec^{-1}]).

Coefficients of lift (C_L) were calculated using steady-state equations ($C_L = 2 \cdot L/(\rho \cdot A_p \cdot U^2)$, where L is total lift, ρ is water density, A_p is planform surface area of the ventral plate of each carapace, and U is water tunnel speed). Pitching moments (M) about the center of mass of the models were computed using the equation: $M = d_1 \cdot (L_2 - L_1) + (L_1 + L_2) \cdot (d_2 \cdot \cos\alpha) + D \cdot (d_2 \cdot \sin\alpha)$, where d_1 is distance between load cell beams in the force balance, d_2 is distance between the center of the force balance and the center of mass of the model, L_1 is lift measured at load cell closest to model, L_2 is lift measured at load cell farthest from model, D is drag on the model, and α is angle of attack of the model. Pitching moment coefficients (C_M) were computed using the equation: $C_M = 2 \cdot M/(\rho \cdot A_p \cdot c \cdot U^2)$, where c = chord length of carapace.

RESULTS

Morphological measurements

There were clear morphological differences in the shapes of the carapaces among the four boxfishes. The spotted boxfish was trapezoidal in cross-section with sharper ventral than dorsal keels (*e.g.*, at maximum girth: mean ventral keel angle = 90.2° ± 13.9 [SD], mean dorsal keel angle = 127.7° ± 5.9), heavily concave sides (at maximum girth: mean concavity = 10.6% S_L ± 1.9) with maximum concavity occurring equidistant between the keels, and convex dorsal/ventral sections (Fig. 1). The trunkfishes were triangular in cross-section with sharp ventral keels (*e.g.*, at the midpoint between maximum girth and the posterior edge of the carapace: ventral keels angles = 33.1 to 43.9°) and concave lateral channeling located approximately 20% of the segmental distance from the ventral to dorsal keels. The smooth trunkfish differed from the buffalo trunkfish in that it had a larger normalized height and width (smooth trunkfish maximum height and width = 41.3% TL ± 1.3 and 35.9% TL ± 2.1, buffalo trunkfish maximum height and width = 35.3% TL ± 1.8 and 23.0% TL ± 8.2), no ornamentation (*i.e.*, no posterior extensions of the ventral keels), and more ventral convexity at the point of maximum girth (smooth trunkfish: 7.4% Sv ± 2.1, buffalo trunkfish: 0% Sv) (Fig. 1). Finally, the scrawled cowfish had a compressed triangular cross-section with a narrow ventral region (maximum width = 19.0% TL ± 9.2) that became significantly concave in posterior locations (13.5% S_v), sides that had significant concavity above the ventral keels in posterior locations (*e.g.*, at the midpoint between maximum girth and posterior edge of carapace: concavity = 6.9% S_L), and a high level of convexity near the dorsal keel along the carapace (*e.g.*, at maximum girth: convexity = 9.2% S_L ± 1.0) (Fig. 1). Furthermore, scrawled cowfish had the most ornamented carapace (*i.e.*, anterior horns and ventral keel extensions) and a center of mass that was located farther forward than in smooth and buffalo trunkfishes (horizontal location of center of mass of scrawled cowfish = 32.3% TL ± 1.0; horizontal location of center of mass of smooth trunkfish and buffalo trunkfish = 37.9% TL ± 2.6 and 39.9% TL ± 2.0, respectively).

DPIV

Although differences in carapace morphology were apparent, vortical flow patterns around the four boxfishes were fairly consistent. For all boxfishes positioned at positive or negative angles of attack, regions of concentrated, attached vorticity began to develop around the ventral keels just posterior to the snout at a longitudinal location corresponding to the eye ridge. These regions of concentrated vorticity intensified posteriorly along the ventral keels, both in terms of peak vorticity and circulation, until two, well-developed counter-rotating vortices ultimately formed at the posterior edge of the carapace (Fig. 2). In general, vortices left the body completely at the caudal peduncle. Some attached, concentrated vorticity also developed dorsally around the eye ridges and was present at the posterior edge of the carapace (Fig. 2).

Peak vorticity and circulation of carapace-induced vortices were lowest at an angle of attack of approximately 0°. As the angles of attack deviated farther from 0°, either in a positive or negative direction, peak vorticity and circulation of vortices intensified. At positive angles of attack, strong vortices consistently formed above the ventral keels within concave channels, while attached regions of vorticity with lower peak vorticity and circulation developed either above

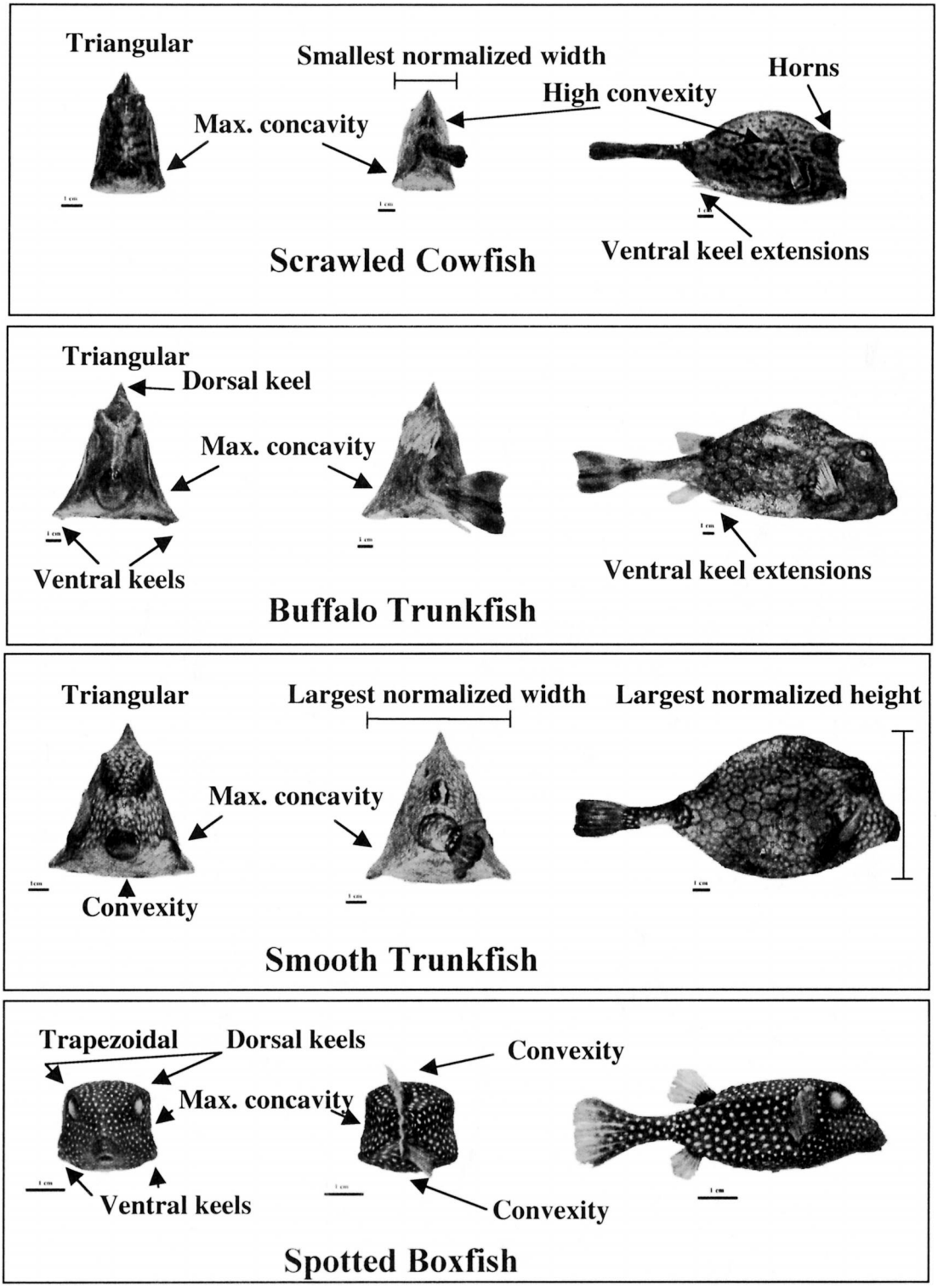

FIG. 1. Anterior, posterior, and lateral views of a scrawled cowfish, buffalo trunkish, smooth trunkfish, and spotted boxfish. Some important features of the different boxfishes are highlighted in the figure. The scale bars represent 1 cm in all images.

or beside the dorsal keel(s) (Fig. 3). At negative angles of attack, vortices formed below the ventral keels, and generally little/no concentrated, attached vorticity developed along/below the dorsal keel(s) (Fig. 3). Irrespective of angle of attack, peak vorticity and circulation of attached ventral vortices were always greatest at the posterior edge of the carapace, which is posterior to the center of mass.

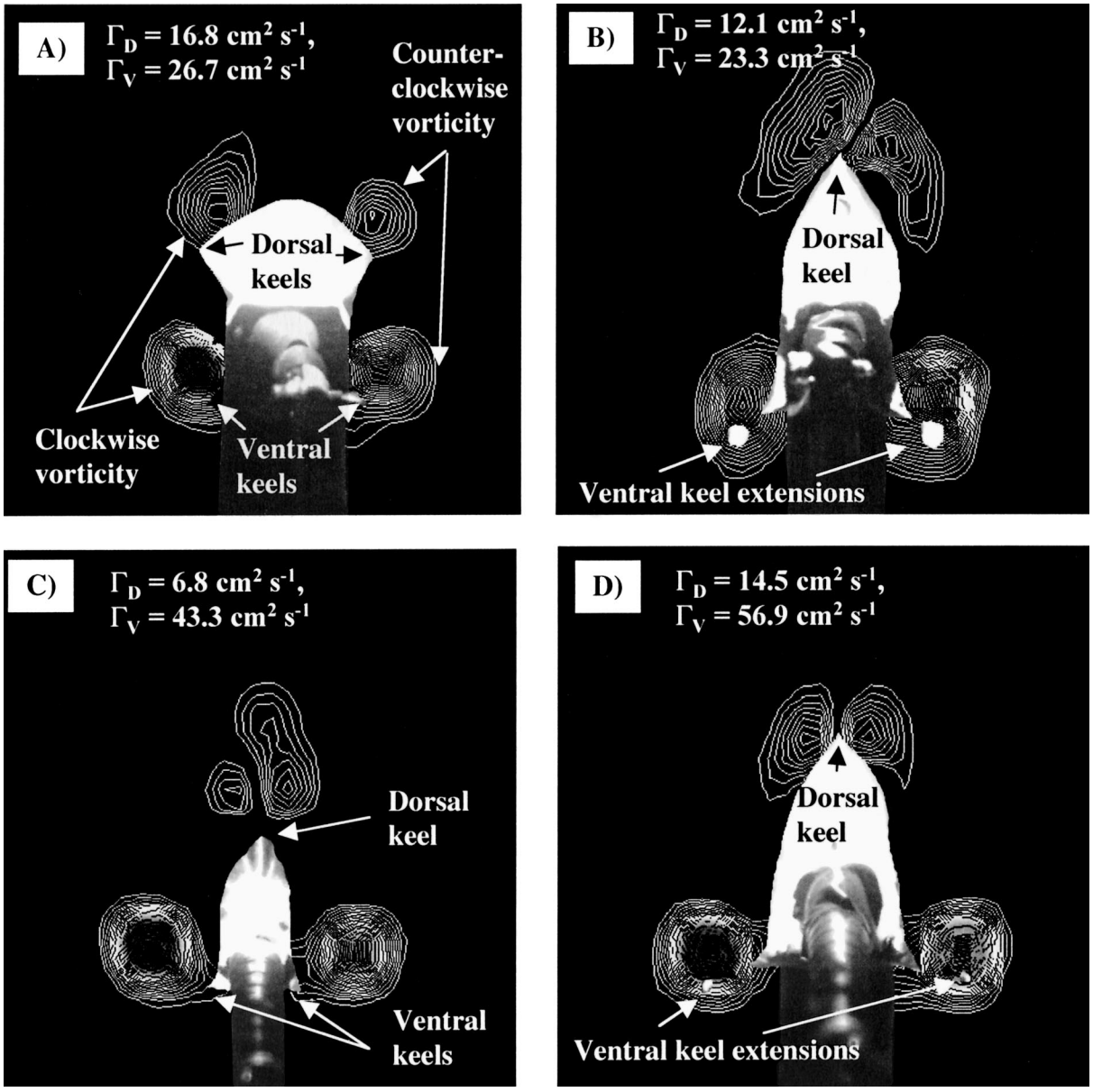

FIG. 2. Vorticity fields around the posterior edge of the carapace of a spotted boxfish (A), scrawled cowfish (B), smooth trunkfish (C), and buffalo trunkfish (D) model positioned at a +10° angle of attack. The vorticity fields are viewed in transverse planes from the rear of the models and are mean results from 30 image pairs. Clockwise vorticity occurs on the left side of the carapaces (both in dorsal and ventral locations), while counterclockwise vorticity occurs on the right side of the carapaces. Shadows underneath the models are areas that were shielded from laser light. Mean circulation magnitude for a dorsal (Γ_D) and ventral (Γ_V) vortex are included in the diagrams.

Pressure measurements

There was a strong correlation between regions of attached, concentrated vorticity observed in DPIV experiments and regions of low pressure detected in pressure experiments. For example, at a positive angle of attack of 10°, regions of concentrated attached vorticity were detected at locations 17 and 21 for the spotted boxfish and locations 34 and 37 for the scrawled cowfish; areas of low pressure also were detected at these locations along dorso-ventral transects (Fig. 4). As angles of attack increased from 0 to 20° or decreased from 0 to −20° and circulation and peak vorticity of regions of concentrated vorticity increased, pressure frequently decreased in these areas (Figs. 4, 5). Moreover, peak regions of low pressure along dorso-ventral transects shifted from above to below ventral keels when changing from positive to negative angles of attack, as was the case for regions of concentrated, attached vorticity (Fig. 5).

Force measurements

For all of the boxfishes, no obvious stall occurred at angles of attack of ±30°, and overall lift coefficients were similar to coefficients of delta wings of similar

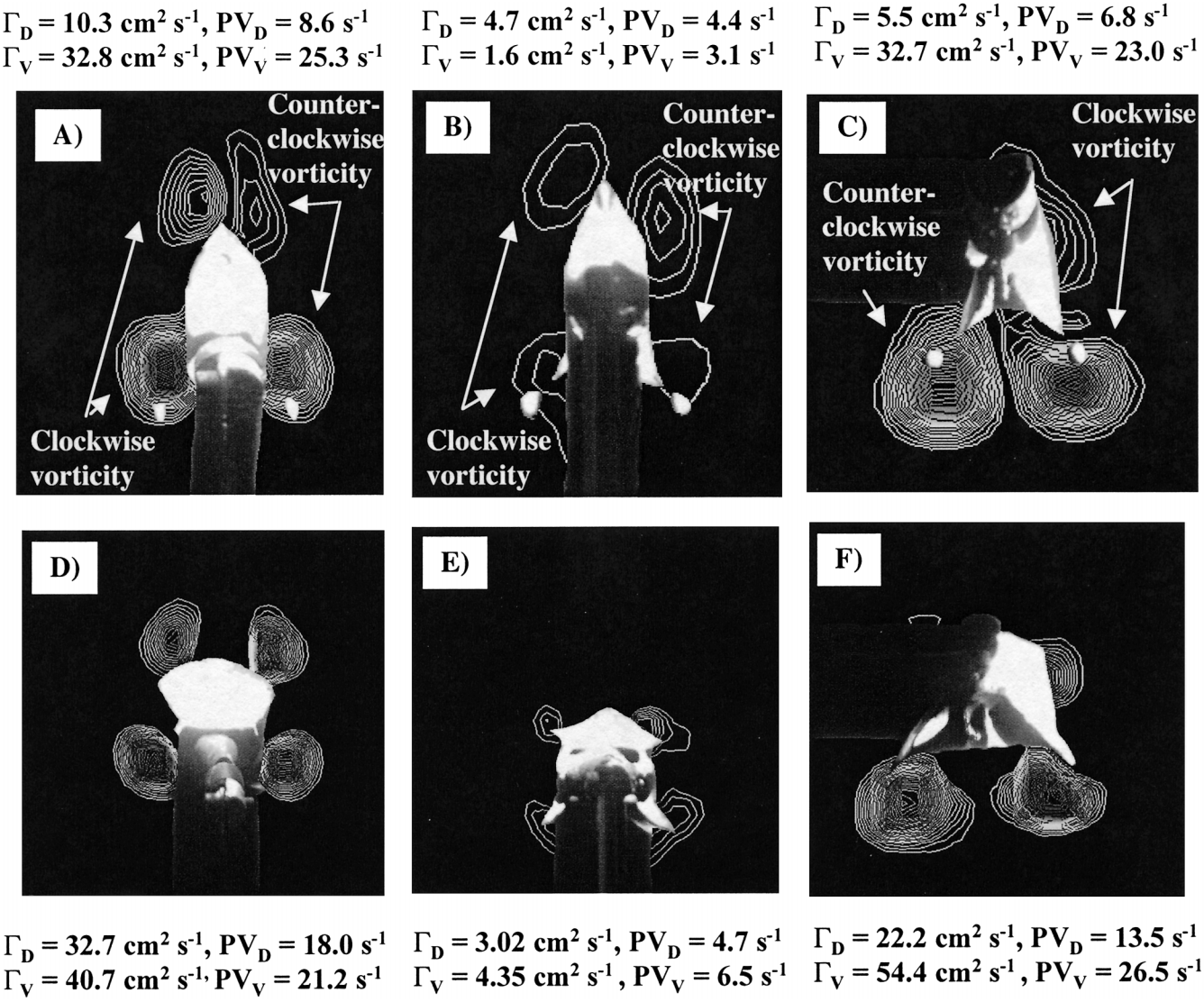

FIG. 3. Vorticity fields around the posterior edge of the carapace of a scrawled cowfish (A–C) and spotted boxfish (D–F) model positioned at angles of attack of +20° (A, D), 0° (B, E), and −20° (C, F). The vorticity fields are viewed in transverse planes from the rear of the models and are mean results from 30 image pairs. At positive and zero angles of attack, clockwise vorticity occurs on the left side of the carapaces (both in dorsal and ventral locations), while counterclockwise vorticity occurs on the right side of the carapaces. At negative angles of attack, flow rotation is reversed; clockwise vorticity occurs on the right side of the carapaces, while counterclockwise vorticity occurs on the left side of the carapaces. Shadows underneath or to the side of models are areas that were shielded from laser light. Mean circulation magnitude for a dorsal (Γ_D) and ventral (Γ_V) vortex and mean peak vorticity magnitude for a dorsal (PV_D) and ventral (PV_V) vortex are included in the diagrams.

aspect ratio. This is demonstrated in Fig. 6, where lift coefficients for the buffalo trunkfish are shown. In general, nose-down pitching moments about the center of mass were detected at positive angles of attack for the different boxfishes, while nose-up pitching moments about the center of mass were detected at negative angles of attack (Fig. 6). The transition angle at which pitching moment coefficients shifted from nose-up to nose-down rotation about the center of mass occurred at ±3° for all four boxfishes.

DISCUSSION

Despite notable differences in cross-sectional and longitudinal body shapes, results from the three inter-related studies indicate that flow patterns around the various carapaces are remarkably similar. DPIV measurements, which provide a global picture of flow around the body, indicate that the ventral keels of the different boxfishes, and to a lesser extent the eye ridges/dorsal keel(s), are all vortex generators. As angles of attack increase from 0° in the positive direction, vortices with stronger peak vorticity and circulation develop along lateral concavities above ventral keels and above or beside dorsal keels, reaching maximum strength at postero-lateral regions of the carapace. As angles of attack increase from 0° in the negative direction, vortices with stronger peak vorticity and circulation develop along ventral concavities below ven-

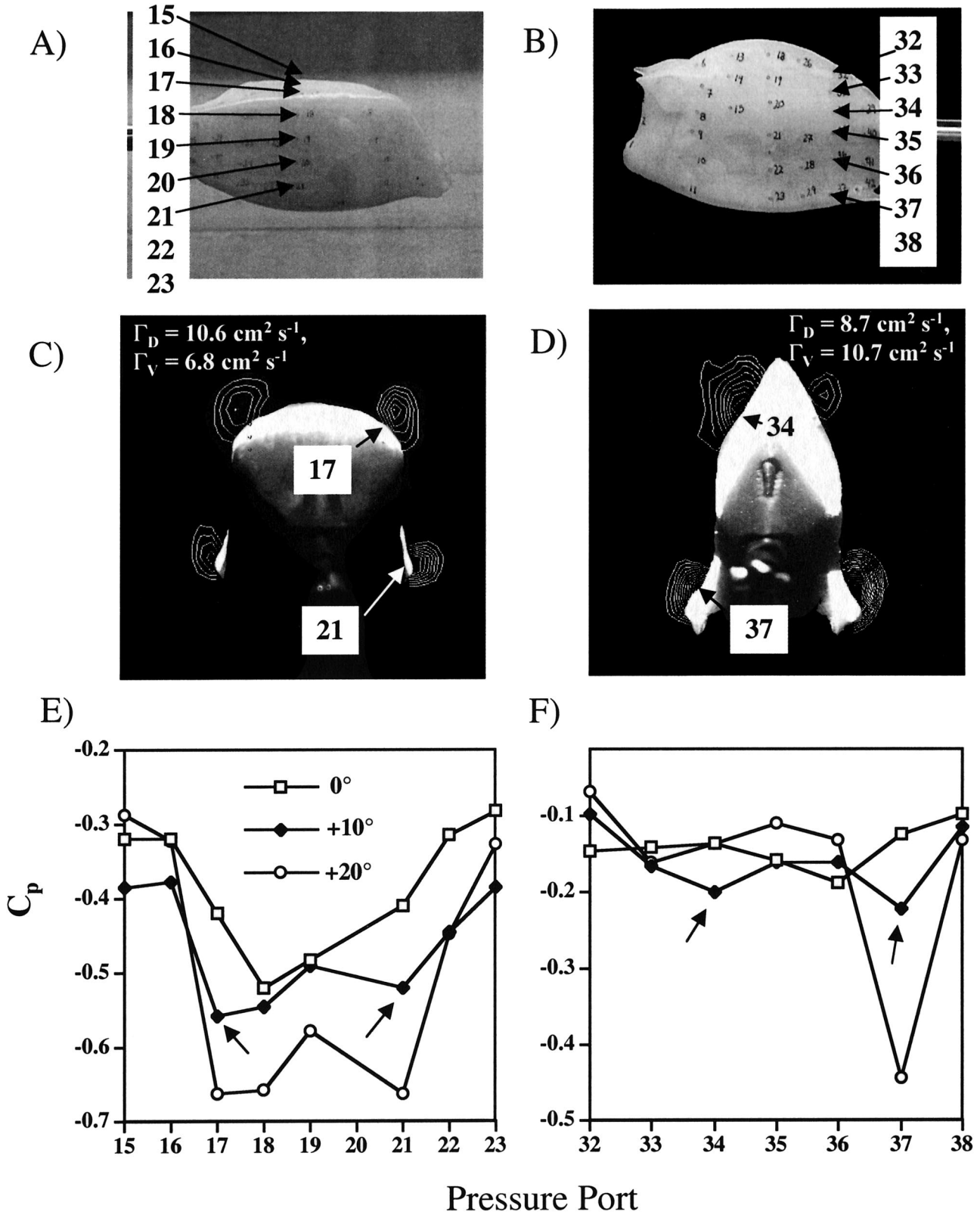

FIG. 4. Pressure ports along a dorso-ventral transect are highlighted for spotted boxfish (A) and scrawled cowfish (B) models. Ports 22 and 23 in (A) and 38 in (B) are located ventrally and are not visible in the lateral views of the models. Mean vorticity fields detected by digital particle image velocimetry at the dorso-ventral transect (viewed in a transverse plane) for spotted boxfish and scrawled cowfish models positioned at a +10° angle of attack are depicted in (C) and (D), respectively. Mean circulation magnitude for a dorsal (Γ_D) and ventral (Γ_V) vortex are included in the diagrams. Pressure coefficients (C_p) along the dorso-ventral transect are illustrated for angles of attack of 0°, +10°, and +20° for spotted boxfish (E) and scrawled cowfish (F). Arrows in pressure graphs highlight C_p at ports illustrated in (C) and (D).

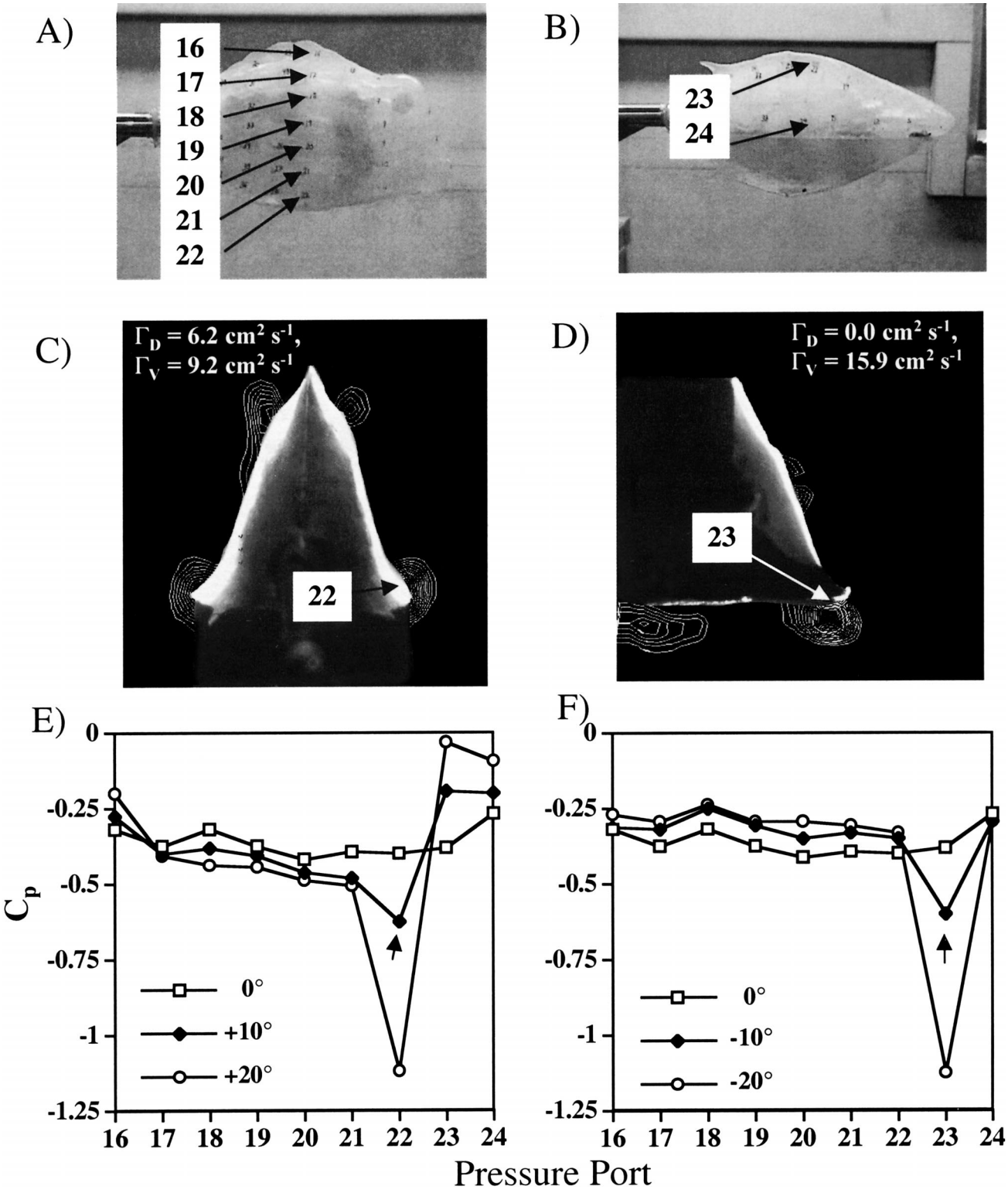

FIG. 5. Pressure ports along a dorso-ventral transect are highlighted in lateral (A) and ventral (B) views of a buffalo trunkfish model. Mean vorticity fields detected by digital particle image velocimetry at the dorso-ventral transect (viewed in a transverse plane) for models positioned at +10° and −10° are depicted in (C) and (D), respectively. Mean circulation magnitude for a dorsal (Γ_D) and ventral (Γ_V) vortex are included in the diagrams. Pressure coefficients (C_p) along the dorso-ventral transect are illustrated for angles of attack of 0°, +10°, and +20° in (E) and 0°, −10°, and −20° in (F). Arrows in pressure graphs highlight C_p at ports illustrated in (C) and (D).

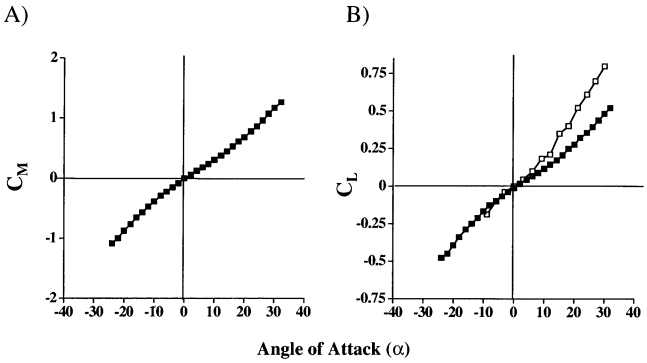

FIG. 6. Pitching moment coefficients about the center of mass (C_M) and lift coefficients (C_L) for a buffalo trunkfish model (shaded squares) positioned at various angles of attack are depicted in (A) and (B), respectively. Positive pitching moment coefficients indicate a nose-down pitching moment about the center of mass, whereas negative pitching coefficients indicate a nose-up pitching moment about the center of mass. In the lift coefficient plot, delta wing coefficients also are depicted as open squares. The delta wing has a similar aspect ratio (0.83) to that of the buffalo trunkfish and the delta wing data are from Schlichting and Truckenbrodt (1969).

tral keels, reaching maximum strength at postero-ventral regions of the carapace.

Pressure measurements, which provide useful information on flow conditions at the surface of the carapace, an area that is difficult to resolve with DPIV, were consistent with global flow patterns observed using DPIV. In regions where attached, concentrated vorticity was observed, regions of low pressure were consistently detected on the carapace surface. Moreover, as angles of attack deviated farther from 0° (either in a positive or negative direction) and circulation of attached vortices increased, pressure dropped accordingly. When used in conjunction, pressure and DPIV data allow us to link global flow features with their concomitant localized effects on the boxfish carapace. An example illustrating the importance of this linkage may be found at the posterior edge of the carapace. In most of the boxfishes, vortex circulation increased from the posterior 3/4 of the carapace to the posterior edge of the carapace, but surface pressures along the carapace did not decrease. The reason for this is that although vortices intensified in strength along the body, the vortex cores actually migrated away from the body and had less impact on localized regions at the surface of the carapace. Consequently, recording both DPIV and pressure data is critical for fully understanding flow effects on the carapace.

Force measurements, which afford an integrative view of the forces acting on the entire carapace, provided further support for the flow patterns detected in DPIV and pressure experiments. Based on DPIV and pressure results, vortices are generated near the anterior of the fish and grow in strength as they move posteriorly down the carapace, most prominently in regions adjacent to ventral keels. Delta wings, which have comparable planforms to boxfishes, produce similar flows. In delta wings a coiled vortex sheet with a core of high vorticity forms at the leading edge of the wing and grows posteriorly along the wing generating lift—a process that differs from lift created through bound circulation in conventional wings and leads to higher angles of attack for stall (Bertin and Smith, 1989). The observed similarity in lift coefficients between delta wings and boxfishes is thus further evidence of vortex generation and subsequent growth along the ventral keels in boxfishes.

The vortical flow patterns summarized here are important for stability development, especially control for pitching, in boxfishes. Attached vortices with the strongest peak vorticity and circulation generally develop posterior to the center of mass and above (positive angles of attack) or below (negative angles of attack) ventral keels that extend laterally at an angle of 0–76° relative to a horizontal axis when viewed in cross-section. Consequently, suction derived from the presence of a vortex above or below the ventral keels should act largely upward and posterior to the center of mass at positive angles of attack (which also occurs in delta wings) and downward and posterior to the center of mass at negative angles of attack. Based on pitching moments recorded in force balance experiments, where nose-down pitching moments occurred and became progressively stronger as angles of attack became more positive and nose-up pitching moments occurred and became progressively stronger as angles of attack became more negative, this is exactly what happens. Therefore, the ventral keels and in some species the dorsal keels are effectively generating self-correcting forces for pitching motions; the degree of self-correction is proportional to the degree to which the fish is perturbed from a horizontal swimming trajectory.

Hove *et al.* (2001) found that boxfishes exhibit some of the smallest amplitude recoil moments known among fishes. As a result they swim in smoother trajectories than either body and caudal fin (BCF) or single-complex median and paired fin (MPF) swimmers. Results from our study indicate that the keeled bony carapace plays an important role in producing this longitudinal stability. Control for pitching is important for fishes, such as boxfishes, that live in highly energetic waters with frequent external disturbances like turbulence. In these environments, effective compensation for perturbations, which can lead to significant displacements and energy-wasting erratic trajectories, is essential for effective and economical swimming (Weihs, 1993; Webb, 2000). Maintenance of smooth swimming trajectories also presumably improves sensory acuity of both hostile and target objects because it reduces complexity of movement, a factor that improves sensory perception in other animals (Land, 1999; Kramer and McLaughlin, 2001).

Each of the three independent but complementary experimental approaches considered in this study provides valuable information about flow patterns around the carapaces of the four morphologically distinct boxfishes. Now that we have an understanding of the hy-

drodynamic properties of the body (yawing experiments also were performed but are not described here), we can separate out the contributions of the body from those of the fins in future studies and examine the complex interaction between the fin movements and body vortex formation in live boxfishes. This will help us better understand how both stability and maneuverability are achieved. These studies will be performed using defocusing digital particle image velocimetry (DDPIV), a new method that allows us to visualize and quantify flows in three dimensions as they move along the body (Pereira *et al.*, 2000, 2002). Given the complex nature of fin movements in boxfishes and the difficulty these movements pose for reconstructing flow around them using 2D DPIV or even stereo-DPIV, the DDPIV approach has tremendous promise and should provide unprecedented data on how fishes swim.

Boxfishes provide a set of nearly unique opportunities for the application of quantitative engineering measurement techniques to the study of the hydrodynamics of swimming in living fishes. As the results summarized here demonstrate, evolution in this group has produced sets of highly sophisticated adaptations to varied environmental conditions these animals must deal with on daily bases. Increased understanding of these properties provides additional opportunities for the development, by humans, of more effective and efficient bioinspired (biomimetic) engineered underwater vehicles.

ACKNOWLEDGMENTS

We thank R. M. Alexander and P. Krueger for valuable intellectual input, M. McNitt-Gray, J. Carnahan, B. Valiferdowsi, and P. Masson for aid during model construction, D. Lauritzen and S. Moein Bartol for assistance during data collection, and D. Dabiri, L. Zuhal, and D. Jeon for technical assistance. Financial support of the Office of Naval Research under contract N00014-96-0607 (to M.S.G. and M. G.) is gratefully acknowledged.

REFERENCES

Bartol, I. K., M. Gharib, D. Weihs, P. Webb, J. Hove, and M. S. Gordon. 2002. Hydrodynamic stability of swimming in ostraciid fishes: Role of the carapace in the smooth trunkfish *Lactophrys triqueter* (Teleostei: Ostraciidae). J. Exp. Biol. (In press)

Bartol, I. K., M. Gharib, P. Webb, D. Weihs, and M. S. Gordon. 2003. Vortical flow generation along the carapaces of morphologically distinct boxfishes: A mechanism for self-correction of recoil motions in ostraciid fishes. J. Exp. Biol. (in review)

Bertin, J. J. and M. L. Smith. 1989. *Aerodynamics for engineers*, 2nd ed. Prentice Hall, Englewood Cliffs.

Blake, R. W. 1977. On ostraciiform locomotion. J. Mar. Biol. Assoc. UK 57:1047–1055.

Blake, R. W. 1981. Mechanics of ostraciiform propulsion. Can. J. Zool. 59:1067–1071.

Blake, R. W. 1983*a*. *Fish locomotion.* Cambridge University Press, Cambridge.

Blake, R. W. 1983*b*. Median and paired fin propulsion. *In* P. W. Webb and D. Weihs (eds.), *Fish biomechanics*, pp. 214–247. Praeger, New York.

Gordon, M. S., J. R. Hove, P. W. Webb, and D. Weihs. 2000. Boxfishes as unusually well-controlled autonomous underwater vehicles. Physiol. Biochem. Zool. 73(6):663–671.

Hove, J. R., L. M. O'Bryan, M. S. Gordon, P. W. Webb, and D. Weihs. 2001. Boxfishes (Teleostei: Ostraciidae) as a model system for fishes swimming with many fins: Kinematics. J. Exp. Biol. 204:1459–1471.

Kramer, D. L. and R. L. McLaughlin, 2001. The behavioral ecology of intermittent locomotion. Amer. Zool. 41:137–153.

Land, M. F. 1999. Motion and vision: Why animals move their eyes. J. Comp. Physiol. A 185:341–352.

Lisoski, D. 1993. *Nominally two-dimensional flow about a normal flat plate.* Ph.D. Diss., California Institute of Technology.

Lorenson, W. E. and H. E. Cline. 1987. Marching cubes: A high resolution 3D surface construction algorithm. ACM Comp. Graph. 21:163–169.

Nelson, J. S. 1994. *Fishes of the world*, 3rd ed. John Wiley and Sons, New York.

Pereira, R., M. Gharib, D. Dabiri, and D. Modarress. 2000. Defocusing DPIV: A 3-component 3-D DPIV measurement technique. Application to bubbly flows. Exp. Fluids 29:S078–S084.

Pereira, R. and M. Gharib. 2002. Defocusing digital particle image velocimetry and the three-dimensional characterization of two-phase flows. Meas. Sci. Technolog. 13:683–694.

Raffel, M., C. E. Willert, and J. Kompenhans. 1998. *Particle Image Velocimetry: A Practical Guide.* Springer-Verlag, Berlin.

Schlichting, H. and E. Truckenbrodt. 1969. Aerodynamik des Flugzeuges, Vol. 2, Ch. 7. Springer-Verlag, Berlin.

Tyler, J. C. 1980. Osteology, phylogeny, and higher classification of the fishes of the order Plectognathi (Tetraodontiformes). NOAA Technical Report NMFS Circular 434:1–422.

Webb, P. W. 2000. Maneuverability versus stability? Do fish perform well in both? 1st International Symposium on Aqua Bio-mechanisms/International Seminar on Aqua Bio-mechanisms. Vol. 1: 21–29.

Weihs, D. 1993. Stability of aquatic animal locomotion. Cont. Math. 141:443–461.

Willert, C. E. and M. Gharib. 1991. Digital particle image velocimetry. Exp. Fluids 10:181–193.